Journal of
Ceramic Science
and Technology

J. Ceram. Sci. Tech., **06** [02] 125-132 (2015)
DOI: 10.4416/JCST2014-00045
available online at: http://www.ceramic-science.com

Additive Manufacturing of Metal-Ceramic-Composites by Thermoplastic 3D-Printing (3DTP)

U. Scheithauer*, T. Slawik, E. Schwarzer , H.-J. Richter, T. Moritz, A. Michaelis

Fraunhofer Institute for Ceramic Technologies and Systems (IKTS) Dresden, Germany
received October 16, 2014; received in revised form December 8, 2014; accepted January 23, 2015

Abstract

In our new approach – thermoplastic 3D printing (3DTP) – high-filled ceramic and metal feedstocks based on thermoplastic binder systems were used to produce metal-ceramic-composites by means of additive manufacturing (AM). The developed AM method has some outstanding advantages compared to other methods. First, the portfolio of applicable materials is not limited. Second, it works almost independently of the properties of the dispersed material.The application of thermoplastic 3D printing with two components is in principle demonstrated with stainless-steel-zirconia composites. Different feedstocks with high powder content up to 50 vol% were prepared. The main challenge was the adjustment of the shrinkage behavior for the different materials, which could be achieved by high-energy milling and the adjustment of the powder content within the metal feedstock. The adapted additive manufacturing method of thermoplastic 3D printing (3DTP) offers new prospects for the fabrication of multi-material components. This AM method will be applicable not only for steel-zirconia composites but also for any other combinations of materials that can be processed to a paraffin-based thermoplastic feedstock and co-sintered.

Keywords: Additive manufacturing, metal-ceramic, thermoplastic, shrinkage, co-sintering

I. Introduction

Additive Manufacturing (AM) is a manufacturing process where objects are built up layer by layer. According to ASTM, additive manufacturing is a "process of joining material to make objects from 3D model data, usually layer upon layer" [1]. The additive manufacturing of polymers is state of the art, and in the field of metals, processing of more and more materials has been achieved. For processing ceramic materials, the technical application of AM technologies has so far been limited. However, ceramic materials have been studied in additive manufacturing processes *ab initio* with the development of the different AM technologies for about 25 years, see e.g. [2,3]. AM technologies can be classified according to the state of the material used [4] – powder materials, liquid materials and solid materials. It is also possible to classify the AM technologies according to the dimensional order [5] – point, line or plane.

All established AM technologies have been tested for ceramic materials. Conventional stereolithography (STL), for example, has been applied for alumina, zirconia, silicon nitride and silica as well as for ZTA-ceramics [6–9]. In this STL-process, a photo-polymerizable ceramic slurry is cured with an UV-laser. Based on the principal approach of using photo-polymerizable binders in the ceramic slurry or paste, specific AM techniques were developed for the production of ceramic green bodies. For example, a robocasting process uses UV-curable inks with high Al_2O_3 loading [10]. Binders that are cured under visible blue light were applied in a DLP (direct light processing) process, which allows the production of complex-shaped dense alumina parts [11]. Selective laser sintering (SLS) was tested for a number of ceramic materials, too [12–16]. 3D powder bed printing is the most commonly used AM process for powder materials. Typical application of 3D powder bed printing focuses on the production of porous ceramic components because of the little compacted powder layers; the green density is too low to reach high density after sintering. However, for a number of applications, high densities are not required, e.g. for bioactive scaffold structures. So scaffold structures based on calcium phosphates [17–21] or porous glass-ceramic [22] have been produced by means of 3D powder bed printing.

In general, when AM methods are used for the production of materials with high sinter density, it is necessary to use a suspension, paste or feedstock with a high powder volume content instead of a dry powder bed. This was shown for example in SLS where, instead of powder layers, suspension layers have been deposited and consolidated (after short drying) with a laser beam [23]. Furthermore, the direct printing of suspensions has been shown to be a promising way to produce dense ceramic materials by means of additive manufacturing [24,25]. Of course, only highly dispersed nano- or submicron-powders can be processed with direct printing using standard printheads.

Conventional fused deposition modeling (FDM) has been tested, for example, to produce functional ceramic materials [26] and alumina [27]. However, the effort for the

* Corresponding author: uwe.scheithauer@ikts.fraunhofer.de; uwe.scheithauer@gmail.com

preparation of the thermoplastic ceramic feedstock in the form of spooled filaments limits FDM application for ceramics.

The robocasting process is computer-controlled deposition of colloidal pastes or slurries. In contrast to original FDM, the carrier fluid is a volatile solvent (water or organic liquid). In robocasting, highly dispersed ceramic suspensions are used for AM of complex ceramic structures [28–29].

Apart from the manifold geometric facilities, which will not be discussed here, some AM techniques have the potential for the production of multi-component materials with three-dimensional space-resolved properties [30].

Our approach aims at the production of two-component parts with high material density. The above-mentioned DLP process has high potential for producing monolithic dense ceramics. However, the production of composite materials is not possible with customary DLP equipment. Despite this, in DLP the material variety is limited because the powder must not absorb light of the wavelength that initiates the photo-polymerization of the binder. Only white or bright powders can be processed. The light absorption of dark powders, e.g. metal powders, prevents the penetration of the light radiation even in thin layers and photo-polymerization cannot start.

The method presented in this paper uses molten, thermoplastic feedstocks that are handled in a dispensing unit with xyz positioning. The feedstocks are based on compositions known from low-pressure injection molding [31,32]. The melting temperature is relatively low (approx. 100 °C) and the viscosity is also relatively low as compared to the thermoplastic feedstocks used in conventional FDM. We use a molten feedstock that, owing to its relatively low viscosity, can be simply dispensed via a thin nozzle. This thermoplastic 3D-printing concept has several advantages. On the one hand, there are no restrictions concerning the applied powder material because consolidation occurs as a result of an increase in viscosity during cooling. On the other hand, composite materials can be produced by using two or more dispensing heads. Basically, it is possible to process all materials that can be dispersed in the molten feedstock.

Former works furnish proof of suitability of the 3DTP for the AM of nearly dense alumina and zirconia components [33], but it has also been possible to process metal powder [34]. By the way, all above-mentioned statements concerning AM of ceramics are also valid in principle for powder metals that are processed to a sinter-metal microstructure (not via melting steps).

In the present paper, the application of this AM process focuses on steel-ceramic composite material. Owing to the combination of steel and ceramic, innovative, multi-functional properties in two and three dimensions can be achieved, such as hard and ductile, electrically or thermally conductive and insulating, magnetic and nonmagnetic. Possible applications are in a variety of industrial and medical fields, for example as cutting tools, wear-resistant components, energy and fuel cell components or as bipolar surgical tools [35–38].

In order to obtain a steel-ceramic composite it is an essential requirement to successfully co-sinter the paired powders in the composite material. As the sintering of the components has to proceed at the same temperature and atmosphere, it is essential that both materials (steel and ceramic) have a comparable sintering temperature. For avoiding critical mechanical stress during cooling, it is also important that the coefficient of thermal expansion of the ceramic and steel material is approximately equal. Differences in the thermal expansion or in the shrinking behavior of the materials can induce high stresses which are the reason for defects such as structural changes, warpage, delamination or cracks [38,39].

Concerning these two afore-mentioned aspects of co-sintering, zirconia and stainless steel are well suited for the composite, which has been verified for example in [40–42]. Thermoplastic 3D printing now offers the potential to produce steel-ceramic composites with high geometric complexity and additionally with the option of three-dimensional graded material properties. The present study evaluates thermoplastic 3D printing for producing steel-zirconia composites in principle. The major challenge is the adaption of the shrinkage behavior of the two materials during co-sintering.

II. Experimental Procedure

(1) Principal setup

Fig. 1 shows the principal setup for thermoplastic 3D printing (3DTP). Heated feedstocks containing a thermoplastic binder matrix and dispersed particles are printed layer by layer. The feedstock immediately solidifies owing to cooling because of the fast heat transfer from the printed feedstock to the underlying layer or to the surrounding atmosphere. Additionally, it is possible to apply the feedstock by micro-dispensing on selected areas, which opens up the possibility to combine different materials or compositions in one layer to achieve a material gradient not only between different layers but within one layer too. More details about the equipment and the process parameters are described further down in this section and in [33,34].

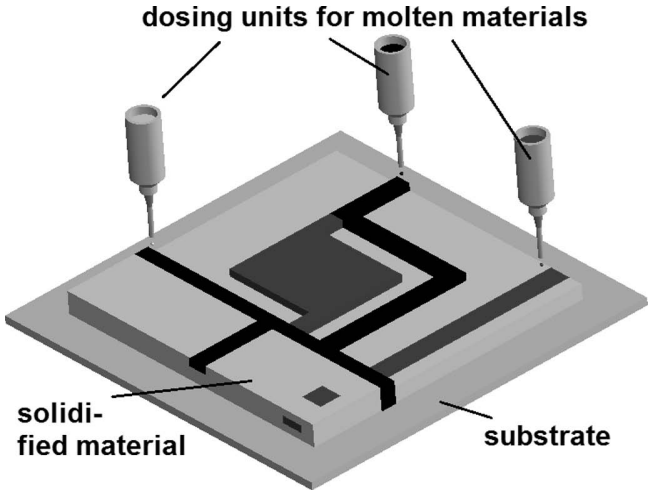

Fig. 1: Scheme of thermoplastic 3D printing (3DTP) for different materials.

(2) Characterization methods

The particle size distribution of the powders was measured with a laser diffraction method (Mastersizer 2000, Malvern Instruments Ltd., UK). Electron scanning microscopy images were used to characterize the shape of the powder particles.

To evaluate the density of the sintered samples, FESEM images were used, too. The FESEM images were converted into binary images, all pores were converted into black pixels and the ceramic or metallic particles into white pixels. The open source software used is called Image J. The software compares the number of black and white pixels, and the porosity in the cross-sectional area can be calculated.

The maximum linear shrinkage was estimated with the help of an optical microscope. An optical dilatometer (Hesse Instruments, Germany) was applied to characterize the shrinkage behavior of the materials during the sintering process. These measurements were all taken in an argon atmosphere with 5 % hydrogen.

(3) Used materials

As ceramic materials, the yttria-stabilized zirconia powders TZ-3Y-E and TZ-3Y-SE (both supplied by TOSOH Corporation, Japan) were used. As steel, the iron-chromium alloy Crofer22APU (-38 µm, ThyssenKrupp VDM, Germany) and 17 – 4 PH (sieved fraction below 12 µm, Sandvik Osprey Powder Group, UK) were used. The materials were chosen because their coefficients of thermal expansion are in the same range [42, 43]. Table 1 shows the particle sizes of the zirconia and steel powders.

The particle size of the ceramic powders is with 0.10 and 0.18 µm (d_{50}) two magnitudes smaller than the particle size of the Crofer22APU (-38 µm) and the 17 – 4 PH powders, which results in higher sinter activity, higher linear shrinkage and a lower reachable powder content in the feedstocks.

The results of dilatometer measurements in Fig. 2 show that the 17 – 4 PH and TZ-3Y-E powders start to sinter 100 K earlier than the TZ-3Y-SE powder. In contrast, the metallic Crofer22APU (-38 µm) powder starts to sinter 150 K later than the TZ-3Y-SE powder. The difference of 250 K between the sintering start of the two metal powders can be explained based on the difference in the melting temperatures and the particle sizes. The sieved 17 – 4 PH powder is a very fine powder for metals, but the ceramic powders are even finer. Nevertheless, sintering starts nearly simultaneously at a comparable temperature to the 17 – 4 PH powder (about 1000°C) because of the higher diffusion rate of metals against zirconia.

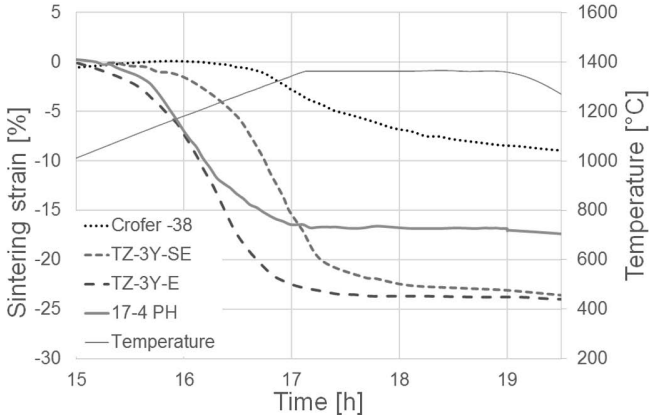

Fig. 2: Dilatometer curves of the starting materials measured under argon atmosphere with 5 % hydrogen [45].

The total linear shrinkage of the ceramic powders (including debinding and sintering shrinkage) are 24 % for TZ-3Y-E and 23 % for TZ-3Y-SE. Compared with the total linear shrinkage of the Crofer (-38 µm) powder, the total shrinkage difference between zirconia and steel is 14 % and 15 % respectively. Because of these differences, adjustment of the sintering behavior of the Crofer22APU-powder was necessary.

Fig. 3 shows another plot of the dilatometer measurements of TZ-3Y-E and 17 – 4 PH. The sintering behavior in the range between 800 °C and 1250 °C is nearly the same. However, at higher temperatures the curves differ and for the maximum shrinkage there is a gap of about 6 %. But in a former study it was shown that the production of defect-free 17 – 4 PH - TZ-3Y-E-samples was possible with multilayer technology and injection molding [43, 44]. Thermoplastic feedstocks were produced for both materials (17 – 4 PH and TZ-3Y-E) to check if it is possible to produce defect-free metal-ceramic-samples by means of 3DTP, too. Reduction of the particle sizes with a high-energy milling step was not performed because the total linear shrinkage should be adjusted for sintering at high temperatures but sintering of the finer 17 – 4 PH would start at lower temperatures than sintering of the TZ-3Y-E powder. The differences in the sintering behavior would be decreased for high temperatures but increased for low temperatures.

The gap between the dilatometer curves of the zirconia materials and Crofer22APU required an adjustment of the sintering behavior for Crofer22APU, which was achieved with high-energy milling. The resulting finer particle size increased the sinter activity with a higher total linear shrinkage and a lower starting temperature. A feedstock was prepared with the milled Crofer22APU powder.

Table 1: Particle size of zirconia and steel powders.

		TZ-3Y-E	TZ-3Y-SE	CroFer22APU (-38 µm)	17-4 PH (-12 µm)
$d_{20,3}$	µm	0,062	0,080	10,9	3,8
$d_{50,3}$	µm	0,105	0,180	24,6	12,2
$d_{90,3}$	µm	0,181	0,362	43,6	29,6

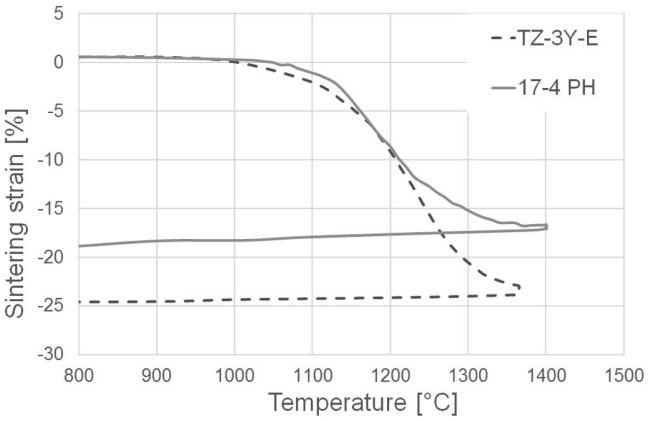

Fig. 3: Dilatometer curves of TZ-3Y-E and 17–4 PH measured under argon atmosphere with 5 % hydrogen.

The densities of the zirconia materials were > 99 % for TZ-3Y-E and > 97 % for TZ-3Y-SE at 1365 °C and > 99.5 % for both powders at a sintering temperature of 1400 °C. The density of the Crofer22APU (-38 µm) after sintering at 1365 °C is about 75 % and at 1400 °C about 87 %. The 17–4 PH powder achieved a density of nearly 100 % already at 1365 °C.

(4) Feedstock preparation

The different zirconia feedstocks were prepared by dispersing the powders in a mixture of molten paraffin and beeswax used as a binder system. The dispersion and homogenization were performed in a heatable ball mill. First the binder system and a dispersing agent were heated up to 100 °C. Then the powder was added to the liquid and dispersed by means of ball milling at 100 °C for 72 h. A powder content of 50 vol% could be achieved.

For preparation of the metal powder feedstocks, a heatable dissolver (Dissolver DISPERMAT CA 20-C, VMA-Getzmann GmbH) was used. After the binder system and a dispersing agent had been heated up to 100 °C, the metal powder was added and the feedstock was homogenized by stirring for 2 h. For the original 17–4 PH powder, a powder content of 47 vol% was adjusted and for the milled Crofer22APU powder a content of 50 vol%.

(5) Manufacturing of the metal-ceramic samples

Laboratory equipment using an xyz-actuating unit with a cartridge fitting was used. The cartridges were moved above a fixed platform. The different feedstocks were funneled in heatable dosing units. Cartridges with fitted dosage needles with diameters between 0.4 mm and 0.8 mm were used. Pressures between 0.2 bar and 4.0 bar had to be applied to deposit the suspension (= liquid feedstock) on a metal tape or a glass slide as the substrate. The temperature of the suspension was about 100 °C .Uniform heating of the cartridge, suspension as well as of the needle is very important as the viscosity of the suspension strongly depends on the temperature. Metal needles with good thermal conductivity were used to avoid clogging. Extra cooling of the platform with the substrate was not required. At room temperature, the suspension solidifies immediately after printing on the substrate or on the previously deposited layer.

(6) Thermal treatment

The green samples were debinded in a powder bed at a very low heating rate, in a first step in air up to 270 °C (heating rate 4 K/h) and then in a second step in Ar atmosphere up to 900 °C (15 K/h). Afterwards the steel-zirconia composites were sintered in an Ar/H_2 atmosphere (80/20) at 1400 °C (3 K/min) for 2 h.

III. Results

(1) Adjustment of sintering behavior

The metallic powder was treated in a high-energy milling step to adapt the sintering behavior of the two materials to each other. Further information about high-energy milling is given in [46, 47]. This milling step yields finer particles, a higher specific surface area, and furthermore a decrease in the crystallite size [47, 48]. As a result of this, the sintering activity is increased, which leads to higher shrinkage (dependent on the green density) and higher density after sintering (compared to the starting powder).

The high-energy milling causes deformation of the spherical starting powder (Fig. 4) to an irregularly and angularly shaped powder (Fig. 5), which could be shown by SEM images of the powders. The bulk density for Crofer22APU decreases from 4 g/cm^3 to 3.1 g/cm^3 and the average particle size from 24.6 µm to 9.4 µm. This packing behavior is more adapted to the behavior of the ceramic material (lower affinity to sedimentation, higher mechanical strength after debinding).

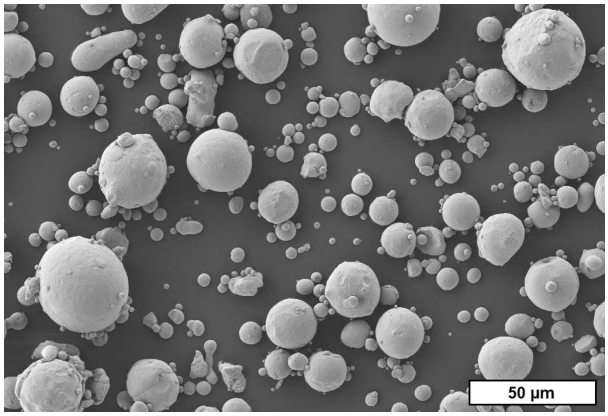

Fig. 4: Electron scanning microscopy images of the spherical starting powder Crofer22APU (-38 µm).

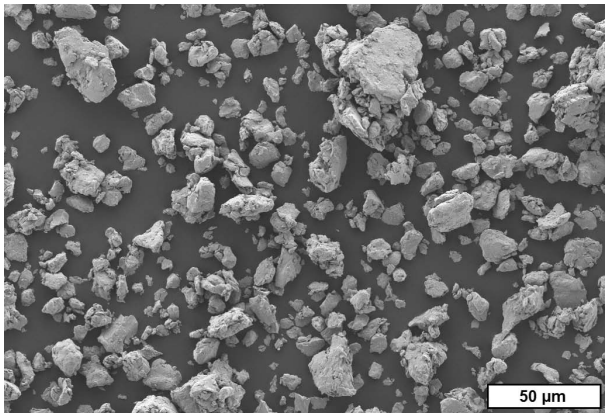

Fig. 5: Electron scanning microscopy images of the high-energy-milled powder Crofer22APU.

Fig. 6 shows the results of dilatometer measurements of the TZ-3Y-SE powder in comparison with the milled Crofer22APU powder. The milled powder starts sintering at the same time as the ceramic one and the shrinkage rate is in the same range, too. Only at the end, there is a slight difference in the total shrinkage of 4 %. This problem can probably be solved by adaption of the green density. The density of the metallic microstructure after sintering at 1400 °C is now above 97 %.

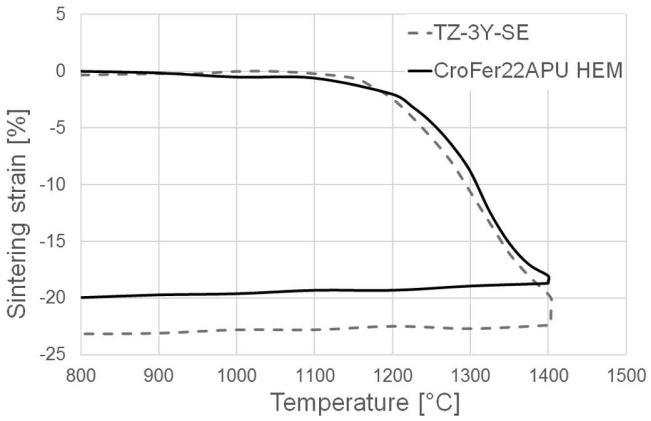

Fig. 6: Dilatometer curves of the milled Crofer22APU powder compared to the TZ-3Y-SE measured under argon atmosphere with 5 % hydrogen.

(2) Sintered samples

Fig. 7 shows the delaminated sample made of 17 – 4 PH and zirconia TZ-3Y-E, Fig. 8 the unimpaired sample made of high-energy milled Crofer22APU and zirconia TZ-3Y-SE. Whereas the metal layers shine, the zirconia looks gray because of the reducing atmosphere during the sintering process.

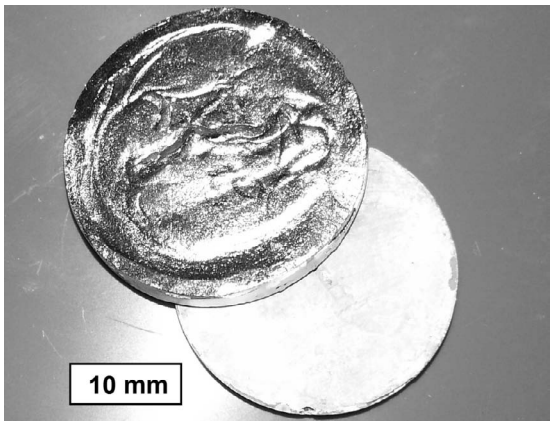

Fig. 7: Delaminated sample made of 17 – 4 PH (left, top) and zirconia (TZ-3Y-E, right).

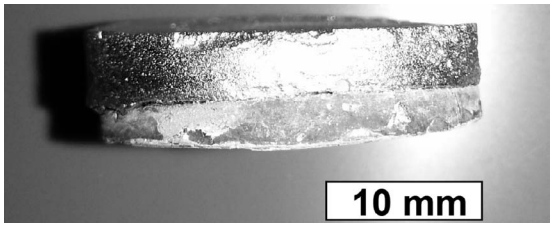

Fig. 8: Unimpaired sample made by 3DTP (zirconia (TZ-3Y-SE) on bottom, milled Crofer22APU on the top).

The differences in the sintering behavior of 17 – 4 PH and TZ-3Y-E at temperatures higher than 1250 °C and in the total linear shrinkage result in a delamination of the two materials. Fig. 7 shows the layers of the two materials, which had the same green diameter after the 3DTP process. After the adjustment of the Crofer22APU powder, it shows nearly the same sintering behavior as the TZ-3Y-SE and the total linear shrinkage of 20 % does not differ very much from the 23 % of the zirconia powder, resulting in a nearly defect-free sample (Fig. 8). Fig. 9 and Fig. 10 show the same results for samples with other shapes made for the two different material pairs.

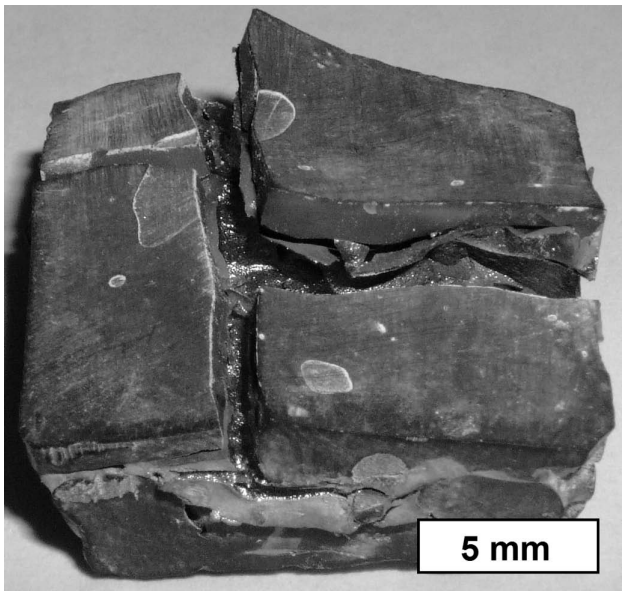

Fig. 9: Destroyed sample made of 17 – 4 PH and TZ-3Y-E.

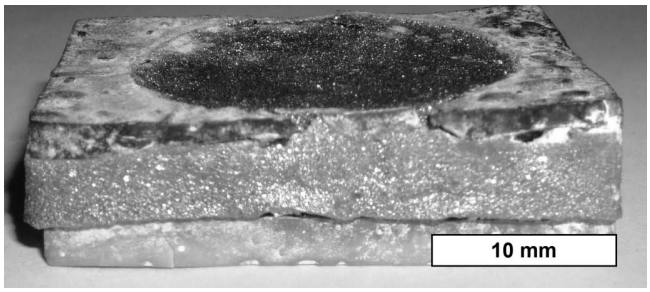

Fig. 10: Samples made of high-energy-milled Crofer22APU and TZ-3Y-SE.

IV. Conclusions

The application of thermoplastic 3D printing with two components is demonstrated in principle by stainless steel-zirconia composites. Different feedstocks with high powder contents up to 50 vol% were prepared. The main challenge was the adjustment of the shrinkage behavior ofthe different materials, which could be achieved by means of high-energy milling and the adjustment of the powder content within the metal feedstock.

After the adjustment of the Crofer22APU powder, critical stresses on the interface between the different materials and delamination could be avoided. Adjustment of the sintering behavior of the 17 – 4 PH powder will follow.

The adapted additive manufacturing method of thermoplastic 3D printing (3DTP) offers new prospects for fabrication of multi-material components. This AM method will be applicable not only for steel-zirconia composites but also for any other combinations of materials that can be processed to a paraffin-based thermoplastic feedstock and then co-sintered.

Acknowledgements

The authors thank Mr Stockmann and Mr Bedrich for preparation of the thermoplastic feedstocks as well as Mrs Frey, Mrs Eichler, and Mr Fesel for the thermal treatment.

References

1 ASTM-Standard F2792 – 12a: Standard terminology for additive manufacturing technologies. March 1, 2012, ASTM International Distributed under ASTM license by Beuth publisher.

2 Lakshminarayan, U., Ogrydiziak, S., Marcus, H.L.: Selective laser sintering of ceramic materials, Proceedings of Solid Free-Form Symposium, 16 – 26, (1990).

3 Lauder, A., Cima, M.J., Sachs, E., Fan, T.: Three-dimensional printing: surface finish and microstructure of rapid prototyped components, *Mater. Res. Soc. Symp. P.*, **249**, 331 – 336, (1992).

4 Chartier, T., Badev, A.: Rapid prototyping of ceramics. In: Handbook of Advanced Ceramics Elsevier, Oxford, UK, 2013.

5 Travitzky, N., Bonet, A., Dermeik, B., Fey, T., Filbert-Demut, I., Schlier, L-, Schlordt, T., Greil, P.: Additive manufacturing of ceramic-based materials, *Adv. Eng. Mater.*, **16**, 729 – 754, (2014).

6 Pham-Gia, K., Rossner, W., Wessler, B., Schäfer, M., Schwarz, M.: Rapid prototyping of high-density alumina ceramics using stereolithography, *cfi/Ber. DKG*, **83**, 36 – 40, (2006).

7 Chartier, T., Duterte, C., Delhote, N., Baillargeat, D., Verdeyme, S., Delage, C., Chaput, C.J.: Fabrication of millimeter wave components via ceramic stereo- and microstereolithography processes, *J. Am. Ceram. Soc.,* **91**, 2469 – 2474, (2008).

8 Griffith, M.L., Halloran, J.W.: Freeform fabrication of ceramics via stereolithography, *J. Am. Ceram. Soc.*, **79**, 2601 – 2608, (1996).

9 Licciulli, A., Corcione, C.E., Greco, A., Amicarelli, V., Maffezzoli, A.: Laser stereolithography of ZrO_2 toughened Al_2O_3, *J. Eur. Ceram. Soc.*, **25**, 1581 – 1589, (2005).

10 de Hazan, Y., Thänert, M., Trunec, M., Misak, J.: Robotic deposition of 3d nanocomposite and ceramic fiber architectures via UV curable colloidal inks, *J. Eur. Ceram. Soc.*, **32**, 1187 – 1198, (2012).

11 Felzmann, R., Gruber, S., Mitteramskogler, G., Tesavibul, P., Boccaccini, A.R., Liska, R., Stampfl, J.: Lithography-based additive manufacturing of cellular ceramic structures, *Adv. Eng. Mater.,* **14**, 1052 – 1058, (2012).

12 Lenk, R., Nagy, A., Richter, H.-J., Techel, A.: Material development for laser sintering of silicon carbide, *cfi/Ber. DKG*, **83**, 41 – 43, (2006).

13 Regenfuss, P., Ebert, R., Exner, H.: Laser micro sintering - a versatile instrument for the generation of microparts, *Laser Technik Journal*, **4**, 26 – 31, (2007).

14 Hagedorn, Y.-C., Wilkes, J., Meiners, W., Wissenbach, K., Poprawe. R.: Net shaped high performance oxide ceramic parts by selective laser melting, *Phys. Proced.*, **5**, 587 – 594, (2010).

15 Wu, Y., Du, J., Choy, K.-L., Hench, L.L.: Laser densification of alumina powder beds generated using aerosol spray deposition, *J. Eur. Ceram. Soc.*, **27**, 4727 – 4735, (2007).

16 Goodridge, R.D., Lorrison, J.C., Dalgarno, K.W., Wood, D.J.: Comparison of direct and indirect selective laser sintering of porous apatite mullite glass ceramics, *Glass Technol.*, **45**, 94 – 96, (2004).

17 Gbureck, U., Hoelzel, T., Biermann, I., Barralet, J., Grover, L.M.: Preparation of tricalcium phosphate/calcium pyrophosphate structures via rapid prototyping, *J. Mater. Sci.: Mater. M.*, **19**, 1559 – 1563, (2008).

18 Seitz, H., Rieder, W., Irsen, S., Leukers, B., Tille, C.: Three-dimensional printing of porous ceramic scaffolds for bone tissue engineering, *J. Biomed. Mater. Res.* B,, **74B,** 782 – 788, (2005).

19 Khalyfa, A., Meyer, W., Schnabelrauch, M., Vogt, S., Richter, H.-J.: Manufacturing of biocompatible ceramic bone substitutes by 3D-printing, *cfi/Ber. DKG*, **83**, 23 – 26, (2006).

20 Deisinger, U., Irlinger, F., Pelzer, R., Ziegler, G.: 3D-printing of HA-scaffolds for the application as bone substitute material, *cfi/Ber. DKG*, **83**, 75 – 78, (2006).

21 Dombrowski, F., Caso, P.W.G., Laschke, M.W., Klein, M., Guenster, J., Berger, G.: 3-D printed bioactive bone replacement scaffolds of alkaline substituted ortho-phosphates containing meta- and di-phosphates, *Key Eng. Mat.*, **529 – 530**, 138 – 142, (2013).

22 Zocca, A, Gomes, C.M., Bernardo, E., Müller, R., Günster, J., Colombo, P.: LAS glass-ceramic scaffolds by three-dimensional printing, *J. Eur. Ceram. Soc.*, **33**, 1525 – 1533, (2013).

23 Sadeghian, Z., Heinrich, J.G., Moztarzadeh, F.: Direct laser sintering of hydroxyapatite implants by layerwise slurry deposition (LSD), *cfi/Ber. DKG*, **82**, E1 – E5, (2004).

24 Cappi, B., Oezkol, E., Ebert, J., Telle, R.: Direct inkjet printing of Si_3N_4: characterization of ink, green bodies, and microstructure, *J. Eur. Ceram. Soc.*, **28**, 2625 – 2628, (2008).

25 Ebert, J., Özkol, E., Zeichner, A., Uibel, K., Weiss, Ö., Koops, U., Telle, R., Fischer, H.: Direct inkjet printing of dental prostheses made of zirconia, *J. Dent. Res.*, **88**, 673 – 676, (2009).

26 Allahverdi, M., Danforth, S.C., Jafari. M., Safari, A.: Processing of advanced electroceramic components by fused deposition technique, *J. Eur. Ceram. Soc.*, **21**, 1485 – 1490, (2001).

27 Bose, S., Darsell, J., Hosick, H., Yang, L., Sarkar, D.K., Bandyopadhyay, A.: Processing and characterization of porous alumina scaffolds, *J. Mater. Sci.: Mater. M.*, **13**, 23 – 28, (2002).

28 Schlordt, T., Schwanke, S., Keppner, F., Fey, T., Travitzky, N., Greil. P.: Robocasting of alumina hollow filament lattice structures, *J. Eur. Ceram. Soc.*, **33**, 3243 – 3248, (2013).

29 Cai, K., Roman-Manso, B., Smay, J.E., Zhou, J., Osendi, M.I., Belmonte, M., Miranzo, P.: Geometrically complex silicon carbide structures fabricated by robocasting, *J. Am. Ceram. Soc.*, **95**, 2660 – 2666, (2012).

30 Polsakiewicz, D., Kollenberg, W.: Process and materials development for functionalized printing in three dimensions (FP-3D), *Refractories WORLDFORUM*, **4**, 1 – 8, (2012).

31 Cetinel, F.A., Bauer, W., Mueller, M., Knitter. R., Hausselt, J.: Influence of dispersant, storage time and temperature on the rheological properties of zirconia-paraffin feedstocks for LPIM, *J. Eur. Ceram. Soc.*, **30**, 1391 – 1400, (2010).

32 Gorjan, L., Dakskobler, A., Kosmac, T.: Strength evolution of injection-molded ceramic parts during wick-debinding, *J. Am. Ceram. Soc.*, **95**, 188 – 193, (2012).

33 Scheithauer, U., Schwarzer, E., Richter, H.-J., Moritz, T.: Thermoplastic 3D Printing — An Additive Manufacturing Method for Producing Dense Ceramics, *JACT*, 1 – 6, (2014).

34 Scheithauer, U., Bergner, A., Schwarzer, E., Richter, H.-J., Moritz, T.: Studies on thermo-plastic 3D printing of steel-zirconia composites, *J. Mat. Res.*, **29**, [17], 1931 – 1940, (2014).

35 Lee, H.C., Potapova, Y., Lee, D.: A core-shell structured, metal-ceramic composite-supported ru catalyst for methane steam reforming, *J. Power Sources*, **216**, 256 – 260, (2012).

36 Molin, S., Tolczyk, M., Gazda, M., Jasinski, P.: Stainless steel/yttria stabilized zirconia composite supported solid oxide fuel cell, *J. Fuel Cell Sci. Technol.*, **8**, 051019 – 1 – 051019 – 5, (2011).

[37] Roberts, H.W., Berzins, D.W., Moore, B.K., Charlton, D.G.: Metal-ceramic alloys in Dentistry: A review, *J. Prosthodont.*, **18**, [2], 188 – 194, (2009).

[38] Largiller, G., Bouvard, D., Carry, C.P., Gabriel, A., Müller, J., Staab, C.: Deformation and cracking during sintering of bi-material components processed from ceramic and metal powder mixes. part I: experimental investigation, *Mech. Mater.*, **53**, 123 – 131, (2012).

[39] Guillon, O., Bordia, R.K., Martin, C.L.: Sintering of thin films/constrained sintering. In: Sintering of advanced materials (ed. Fang, Z. Z.), Woodhead Publishing, 2010.

[40] Yeo, J., Jung, Y., Choi, S.: Zirconia-stainless steel functionally graded material by tape casting, *J. Eur. Ceram. Soc.*, **18**, 1281 – 1285, (1998).

[41] Dourandish, M., Simchi, A., Shabestary, E.T., Hartwig, T.: Pressureless sintering of 3Y-TZP/stainless-steel composite layers, *J. Am. Ceram. Soc.*, **91**, 3493 – 3503, (2008).

[42] Dourandish, M.A., Simchi, A.: Study the sintering behavior of nanocrystalline 3Y-TZP/430L stainless-steel composite layers for co-powder injection molding, *J. Mater. Sci.*, **44,** 1264 – 1274, (2009).

[43] Baumann, A., Brieseck, M., Höhn, S., Moritz, T., Lenk, R.: Developments in multi-component powder injection moulding of steel-ceramic compounds using green tapes for inmould label process, *Powder Injection Moulding International*, **2**, [1], 55 – 58, (2008).

[44] Baumann, A., Moritz, T., Lenk, R.: Inmould labelling – a new process variant of the multicomponent powder injection moulding for the production of material composites, Techn. Keram. Werkstoffe, Kap. 3.4.8.8, 123. Erg.-Lfg. Juli 2011 (in german).

[45] Slawik, T., Bergner, A., Puschmann, R., Franke, P., Raethel, J., Behnisch, T., Scholl, R., Berger, L.-M., Moritz, T., Zelm, R., Gude, M., Michaelis, A., Beyer, E., Leyens, C., Grossmann, H., Kieback, B.: Metal-ceramic layered materials and composites manufactured using powder techniques, *Adv. Eng. Mater.*, **16**, [10], 1293 – 1302, (2014).

[46] Scholl, R., Dinh, L.N., Fister, D., Spieker, C.: Processes for the manufacture of fine metal, Alloy and Composite Powders,(in German), German patent, DE10331785, filed on 11.07.2003.

[47] Scholl, R.: New powders for high-alloy sintered materials, (in German), Proceedings of 24th Hagen Symposium on Powder Metallurgy, (2005).

[48] Kiran, U.R., Kumar, M.P., Sankaranarayana, M., Singh, A.K., Nandy, T.K.: High energy milling on tungsten powders, *Int. J. Refract. Met. H.*, **48**, 74 – 81, (2015), pre-published online.